Rapid quenching and properties of hard magnetic materials in MnAl–X (X = Ti, Cu, Ni, C, B) systems

Y. SAKKA, M. NAKAMURA*, K. HOSHIMOTO
*National Research Institute for Metals, 3–12, Nakameguro-2, Nakameguro-ku, Tokyo 153, Japan; *National Research Institute for Metals, Tsukuba Laboratories, Sengen, Tsukuba, Ibaraki 305, Japan*

MnAl–X (X = Ti, Cu, Ni, C, B) ribbons were fabricated by a rapid quenching from the melt using a single roller method. As-rapid quenched ribbons were quenched completely into high temperature h c p phase. The rapid quenched ribbons were brittle especially carbon doped ribbons, however, the titanium doped ribbons were relatively ductile. Hard magnetic properties were measured using a vibrating sample magnetometer for the ten kinds of ribbons annealed at 410–700° C for 10 min–100 h. Phase transformation characteristics and magnetic properties were discussed by comparison with the samples produced by the conventional method. Titanium, boron and carbon doped ribbons showed good hard magnetic properties.

1. Introduction

The ferromagnetic π phase ($L1_0$ structure) in MnAl has a face-centred tetragonal structure and is highly anisotropic with the easy axis of magnetization in the [0 0 1] direction [1]. This π phase is meta-stable phase [2] as shown in Fig. 1 [3]. This metastable phase has been produced in several ways, e.g. either by quenching the high temperature ε phase (h c p A_3 structure) followed by an anneal below 600° C, or by cooling the ε phase at rates of the order of 0.5° C sec^{-1} [4]. In the former method, the quenching rate is not so fast that small stable phase occurs. In the latter method, it is difficult to control the cooling rate. Koch [2] and others developed processes for Mn–Al permanent magnets but industry did not produce the alloy. Recently carbon addition was discovered to stabilize the π phase and to enhance its workability. It appears that the addition of carbon limits the grain growth and thus the grain size to approximately 1 μm, making the material more ductile [5, 6]. However, warm extrusion is a difficult process requiring heavy machines and therefore large capital investment [7].

The melt quenching technique has a large merits from the fabrication process and structural standpoints. It is possible to produce materials directly from the liquid state and to obtain the as-quenched phase including various features such as refinement of grain size, non-equilibrium phase or suppression of segregation, and others [8].

Several authors had previously studied the properties of Mn–Al or Mn–Al–C magnets produced by rapid quenching techniques [9–11]; however, the transformation process had not been ascertained, and the effect of introducing other elements into Mn–Al had not been studied. The purpose of the present paper is to study the features of the transformation of the rapid quenched samples compared with the samples prepared by the conventional method, and the effect of doping X elements (X = Ti, Cu, Ni, C, B) into the Mn–Al alloy.

2. Experimental details

Commercially pure Mn, Al and X (X = Ti, Cu, Ni, C, B) were melted by a high-frequency or an arc furnace in an argon atmosphere. The alloys were subsequently heat treated for 2 h at 1100° C and rapidly quenched in water. The atomic fractions determined by chemical analysis are shown in Table I. The rapid

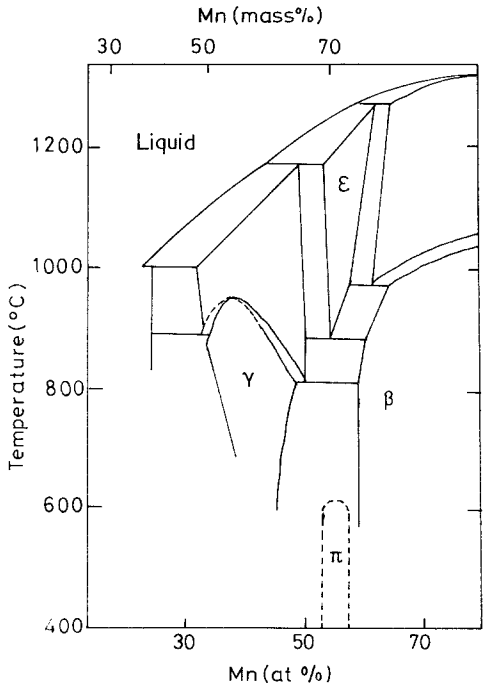

Figure 1 Portion of the Mn–Al phase diagram.

0022–2461/89 $03.00 + .12

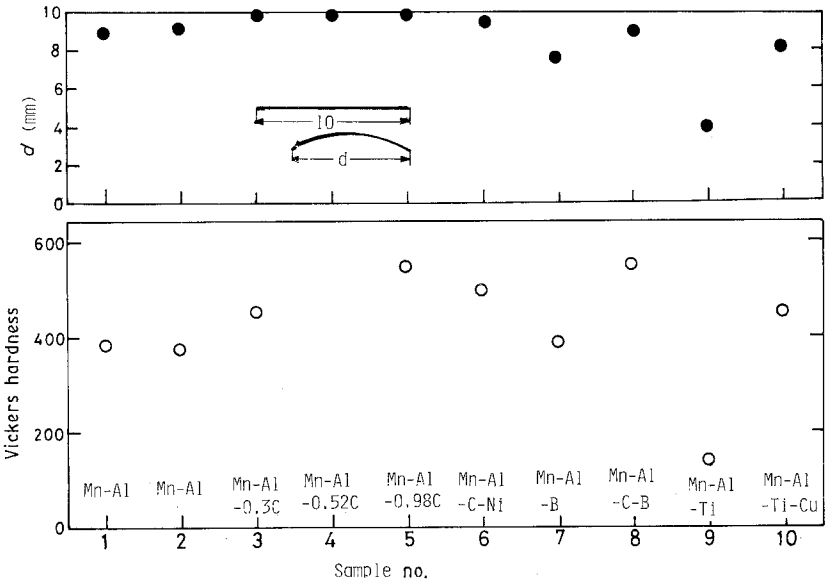

Figure 2 Mechanical properties of the rapidly quenched ribbons, where the sample No. corresponds to Table I.

quenching apparatus used for these experiments consisted of a rotating iron disk of 8 cm in diameter. A charge of approximately 3 g was placed into silica crucible having a nozzle of 0.9 cm in diameter, and melted by a platinum furnace at 1400° C. The molten materials were spurted onto the rapidly rotating roller through the nozzle by the aid of rapid increase in argon pressure in the silica crucible. Vaporization upon melting was not excessive because of an oxide skin which formed over the surface [9].

The mechanical properties of the as-quenched ribbons were examined by micro-Vickers hardness and simple bending test. Micro-Vickers hardness was conducted at the load of 100 gf, and five measurements were averaged. The water quenched alloys and the rapid quenched ribbons were annealed at temperatures of 410–700° C for 10 min–100 h in a vacuum. The structures of the specimen were examined by optical microscopy, scanning electron microscopy (SEM) and X-ray diffraction using filtered Cu$K\alpha$ radiation. The variation of the magnetization with induction up to 13 kOe was measured in a vibrating sample magnetometer. Measurements were made both water quenched samples (defines bulk samples) and rapid quenched ribbons at room temperature.

3. Results and discussion

3.1. Rapid as-quenched ribbons

The rapidly quenched ribbons were obtained in the conditions of a rotating roller speed of 6200 r.p.m. and an argon pressure of 0.6 kg cm^{-2}. X-ray diffraction examination of the rapidly quenched ribbons revealed that the Mn–Al–X (X = Ti, Cu, Ni, C, B) were quenched completely into the high temperature h c p phase and that no diffraction patterns attributable to any other phases were presented. The micro-Vickers hardness and bending length are shown in Fig. 2. The ribbons which had been cut into 10 mm were slowly bent by fixing one end of the ribbons, and the bending length d was measured when the ribbons were fractured. The rapidly quenched ribbons were brittle, especially the carbon doped samples; however, the titanium doped Mn–Al ribbons were relatively ductile. As the examples of the fractured surface of the as-quenched ribbons, Fig. 3 shows the SEM photographs of the brittle Mn–Al–C (No. 5 in Table I) and the ductile Mn–Al–Ti (No. 9) ribbons. Both as-quenched ribbons exhibited intergranular fracture and transgranular cleavage fracture, and showed no significant microstructural differences. The ductility of the titanium added Mn–Al ribbons seems attributed to the low hardness. Since the workability is one of the most important factors of the hard magnetic materials, the titanium doped Mn–Al ribbon is superior.

3.2. Magnetic properties

The variation of the magnetization with induction up to 13 kOe was measured in a vibrating sample magnetometer. Measurements were made of both water-quenched samples and rapidly quenched ribbons. Figure 4 shows the typical hysteresis loops of magnetization against induction of the rapid quenched

TABLE I Chemical analysis of specimens

Sample no.	Mn	Al	C	B	Ti	Cu	Ni
1	70.60	29.40	–	–	–	–	–
2	69.26	30.74	–	–	–	–	–
3	69.30	30.40	0.30	–	–	–	–
4	70.00	29.48	0.52	–	–	–	–
5	70.60	28.42	0.98	–	–	–	–
6	69.40	29.40	0.54	–	–	–	0.66
7	70.80	27.73	–	1.47	–	–	–
8	69.50	29.29	0.46	0.75	–	–	–
9	69.70	28.54	–	–	1.76	–	–
10	68.30	28.90	–	–	1.90	0.90	–

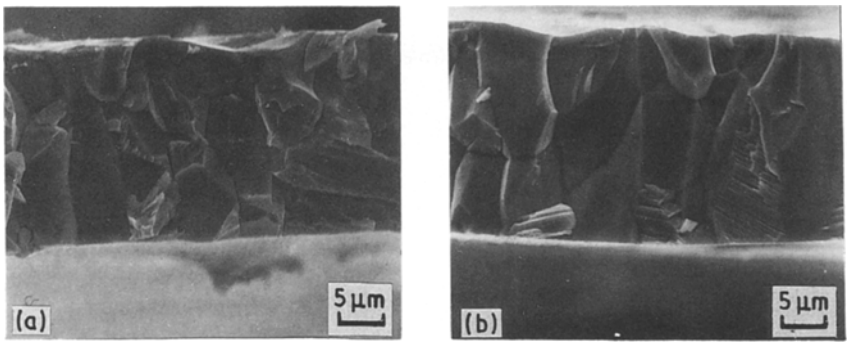

Figure 3 SEM photographs of the fractured surface of the rapidly quenched ribbons. (a) C-doped ribbon (No. 5), (b) Ti-doped ribbon (No. 9).

ribbons of Mn–Al–C (No. 3 in Table I) annealed at 410° C for 5 h. The hysteresis loops of the ribbons measured both parallel and perpendicular to the ribbon axis were equal; therefore, there is no contribution arising from preferred crystallographic orientation, which was also confirmed by X-ray diffraction measurements. Randomly oriented material is a characteristic of the rapid quenched material [9].

3.2.1. Mn–Al systems

Figures 5 and 6 show the magnetization measured at 13 kOe coercive force $B_{13\,kOe}$, remanence B_r and coercive force H_c as function of annealing time at a fixed temperature for the rapid quenched Mn–Al ribbons (Nos 1 and 2). Figure 7 shows the hard magnetic properties for the water-quenched bulk Mn–Al (No. 2). A small variation of manganese concentration has little effect on the magnetic properties in this experimental range as seen in Figs 5 and 6. The rapidly quenched ribbons show better magnetic properties than the water-quenched bulk samples as seen by comparison of Fig. 6 with Fig. 7. Table II shows the structure of the rapidly quenched 70.6 Mn–Al ribbons, where the values in brackets denote the X-ray intensity ratio of π (0 0 2) to β (1 1 1). The decrease of magnetization B and coercive force H_c corresponds to transformation of π phase to β phase. The transformation of ε phase to π phase is known to occur by the following two steps [4]. First it goes through an ordering process to form ε' phase, with an orthorhombic structure (B19-type), which then goes on to form π phase by martensitic transformation. The transformation of the high temperature ε phase, which is quenched by rapid quenching, to π phase is relatively fast in the Mn–Al systems, and the water quenched bulk samples already π phase before annealing. The transformation of π phase to β phase is relatively slow and the transformation in Bulk sample is slower than that in the rapidly quenched ribbons as seen by comparison of Fig. 6 with Fig. 7. And also H_c is greater for the rapidly quenched ribbons than that for the bulk samples. These differences are considered to arise from the grain size difference or defect concentration difference [17], where the rapid quenched ribbons had smaller grain size and larger defect concentration.

3.2.2. Mn–Al–C(Ni) systems

Figures 8 to 10 show the relation between tempering time and the magnetic properties of the rapid quenched

TABLE II Phases observed in 70.6 Mn–Al and 70.6 Mn–Al–0.98 C ribbons

Annealing		70.6 Mn–Al		70.6 Mn–Al–0.98 C phases
temperature	time	Phases	[π (0 0 2)/β (1 1 1)]	
Rapidly as-quenched		ε		ε
410 (° C)	1 (h)	π		ε
410	2	$\pi + \beta$	[15.0]	ε
410	5	$\pi + \beta$	[11.9]	$\varepsilon + \pi$
410	10	$\pi + \beta$	[6.7]	$\varepsilon + \pi$
410	20	$\pi + \beta$	[5.4]	$\varepsilon + \pi$
410	50			π
460	1	$\pi + \beta$	[7.3]	π
460	2	$\pi + \beta$	–	π
460	5	$\pi + \beta$	[10.2]	π
460	20	$\pi + \beta$	[5.4]	$\pi + \beta$
530	1	$\pi + \beta$	[4.4]	π
530	2	$\pi + \beta$	[4.4]	π
530	5	$\pi + \beta$	[2.3]	$\pi + \beta$
600	1	$\pi + \beta$	[1.8]	π
600	2	$\pi + \beta$	[1.6]	$\pi + \beta + Mn_3AlC$
600	5	$\pi + \beta$	[1.1]	$\pi + \beta + Mn_3AlC$
700	1	β		$\pi + \beta + Mn_3AlC$

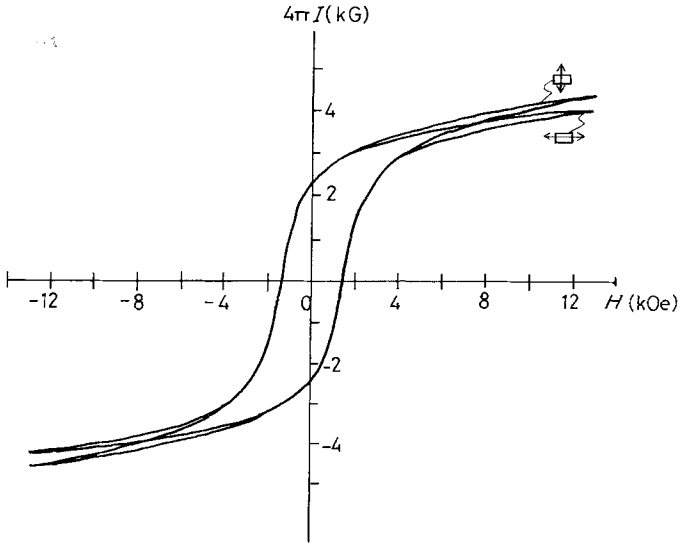

Figure 4 Magnetization against induction loops of Mn–Al–C (No. 3) ribbon annealed at 410° C for 5 h, parallel and perpendicular to ribbon axis.

MnAl–C (Nos. 3–5) ribbons. Within the carbon solubility limit, which is approximately 0.4 mass % in 70 mass % Mn–Al systems [5], the relation between tempering time and the magnetic properties of Mn–Al–C ribbons are similar to that of the undoped Mn–Al ribbons as seen by comparison of Fig. 8 with Figs 5 and 6. The phase transformations of both ε phase to π phase and π phase to β phase were retarded by the carbon doping beyond the solubility limit as seen in Table II and Figs 9 and 10. These results suggest that the transformations were depressed by the Mn_3AlC precipitates, which were observed annealed for a long time or at high temperatures by X-ray diffraction as shown in Table II.

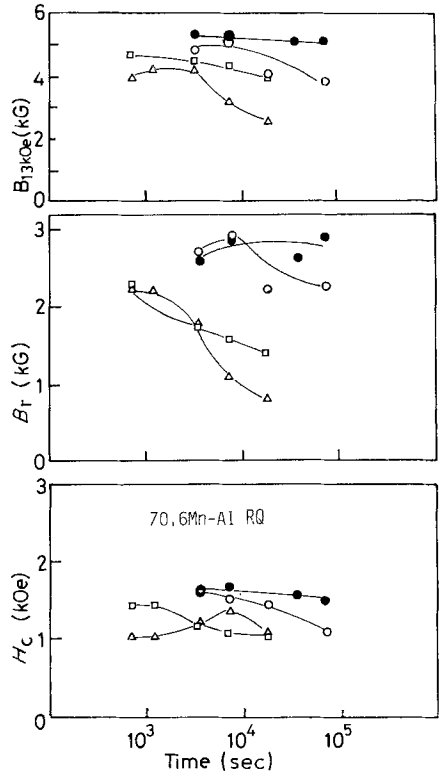

Figure 5 Relation between tempering time and magnetic properties of the rapidly quenched 70.6 Mn–Al ribbons, where $B_{13\,kOe}$, B_r and H_c denote the magnetization measured at 13 kOe, remanence and coercive force, respectively. (●) 410°C, (○) 460°C, (□) 530°C, (△) 600°C.

It has been known that additional doping of nickel increases the coercive force in the extruded sample [6]. Figure 11 shows the magnetic properties of the nickel doped Mn–Al–C rapidly quenched ribbons (No. 6), where nickel addition does not effect significantly the magnetic properties and the rate of transformation of the Mn–Al–C. Since the mechanical properties were slightly improved by nickel addition as seen in Fig. 2, nickel doping is effective for magnet materials.

Figure 12 shows the magnetic properties of the water-quenched 70.0 Mn–Al–0.52C (No. 4) bulk samples. By comparison of Fig. 9 with Fig. 12, it is also seen that quenching rate does not affect the magnetic properties and the transformation rate, probably because of Mn_3AlC precipitates, which depress the grain growth. The higher coercive force may result

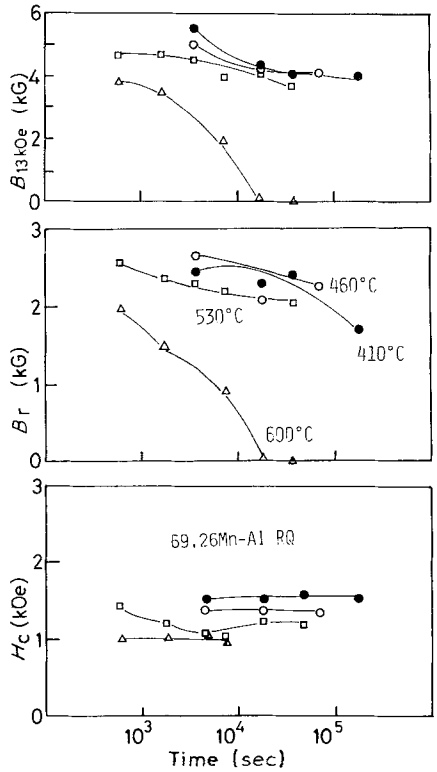

Figure 6 Relation between tempering time and magnetic properties of the rapidly quenched 69.26 Mn–Al ribbons. (●) 410°C, (○) 460°C, (□) 530°C, (△) 600°C.

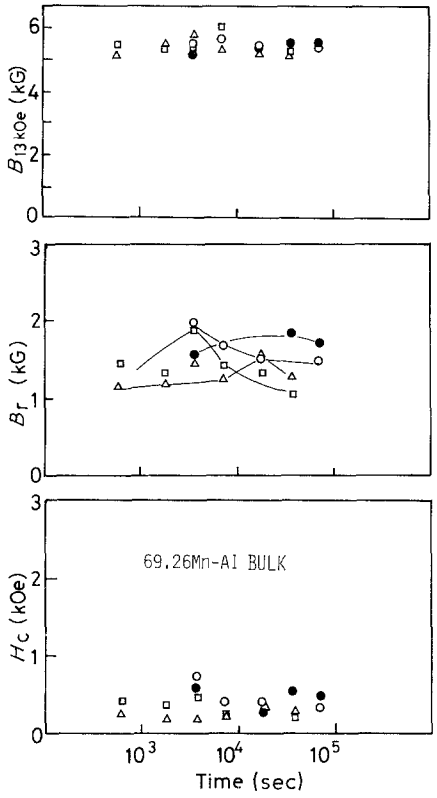

Figure 7 Relation between tempering time and magnetic properties of the water-quenched 69.26 Mn–Al bulk samples. (●) 410°C, (○) 460°C, (□) 530°C, (△) 600°C.

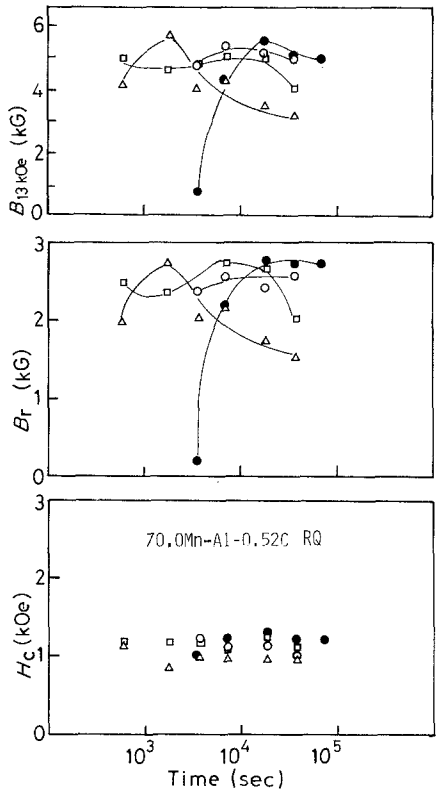

Figure 9 Relation between tempering time and magnetic properties of the rapidly quenched 70.0 Mn–Al–0.52 C ribbons. (●) 410°C, (○) 460°C, (□) 530°C, (△) 600°C.

from increased domain-wall pinning by the carbides and reduction of grain size by carbides [11, 17].

3.2.3. Mn–Al–B(C) systems

Figure 13 shows the relation between tempering time and the magnetic properties of the rapidly quenched 70.8 Mn–Al–1.47B (No. 7) ribbon. Boron-doped Mn–Al ribbons have a relatively large value of H_c; however, the tempering time dependences of H_c are greatly different from those of the other ribbons. The H_c increases as tempering time increases in the boron-doped MnAl.

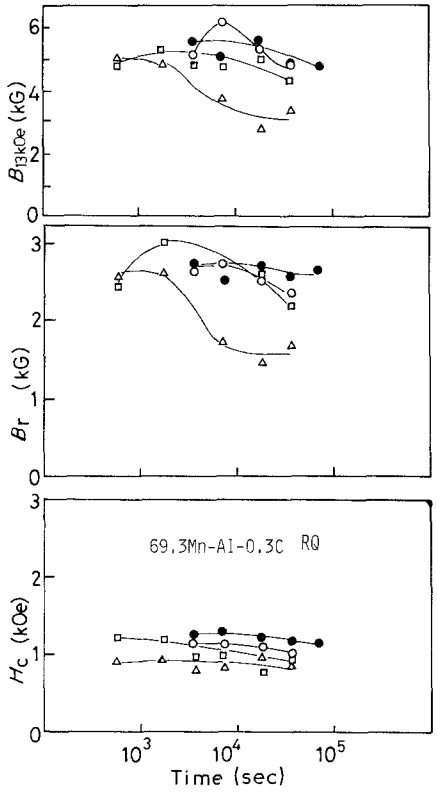

Figure 8 Relation between tempering time and magnetic properties of the rapidly quenched 69.3 Mn–Al–0.3C ribbons. (●) 410°C, (○) 460°C, (□) 530°C, (△) 600°C.

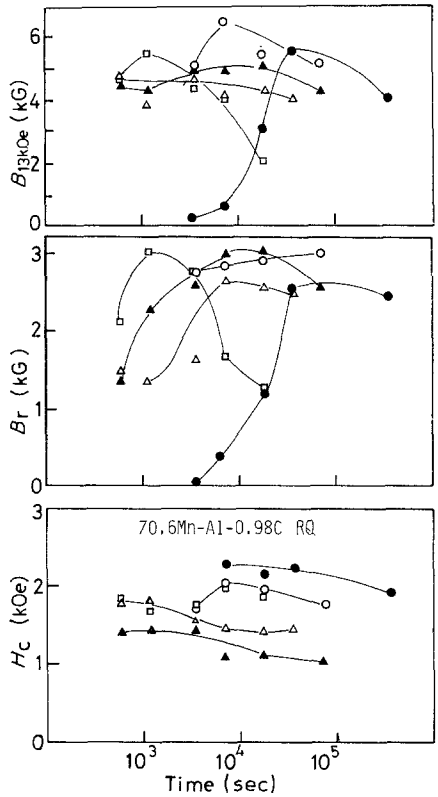

Figure 10 Relation between tempering time and magnetic properties of the rapidly quenched 70.6 Mn–Al–0.98 C ribbons.

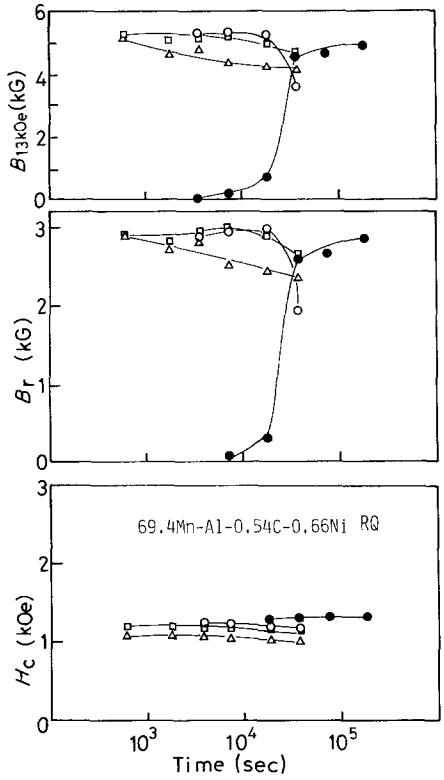

Figure 11 Relation between tempering time and magnetic properties of the rapidly quenched 69.4 Mn–Al–0.54C–0.66Ni ribbons.

Kamino *et al.* [12, 13] reported that needle like precipitate was observed by doping boron above 2 mass %, and they suggested that boron doped alloys consisted of the other hard magnetic and soft magnetic phases by the hysteresis loops which showed a snaky form. In the present rapidly quenched ribbon, the unknown phase was also observed by X-ray diffraction patterns for the long annealed ribbons. The

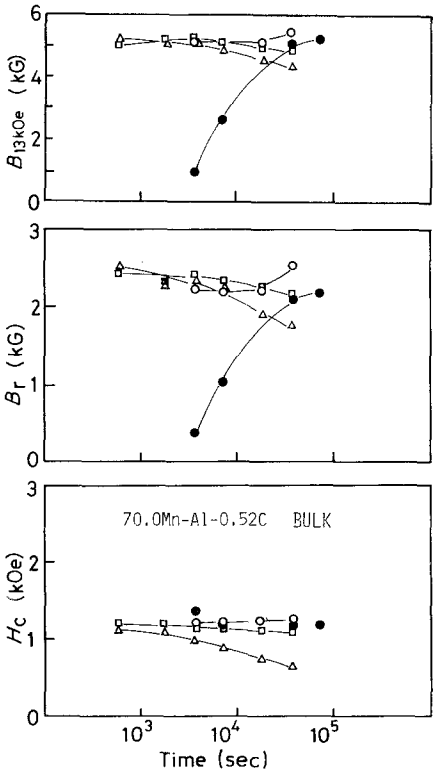

Figure 12 Relation between tempering time and magnetic properties of the water-quenched 70.0Mn–Al–0.52 C bulk samples.

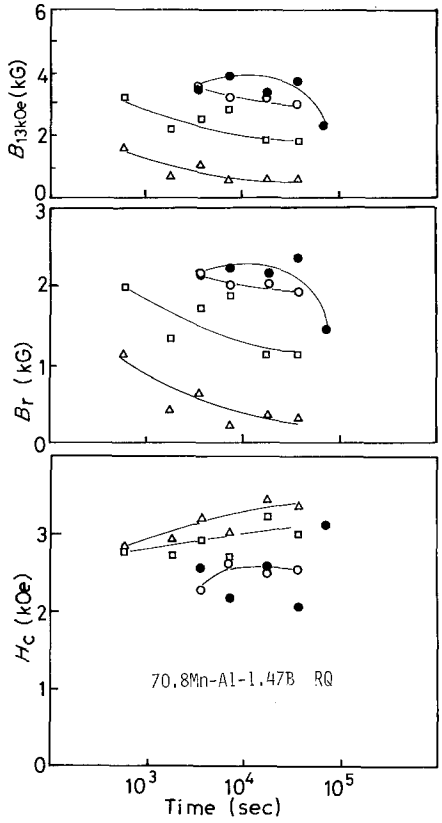

Figure 13 Relation between tempering time and magnetic properties of the rapidly quenched 70.8 Mn–Al–1.47B ribbons.

different relations between tempering time and H_c suggest that another hard magnetic phase is produced during tempering in the Mn–Al–1.47 B ribbons.

To increase the B_r in the Mn–Al–B systems, carbon doping was tried. Figure 14 shows the results of rapidly quenched 69.5 Mn–Al–0.46C–0.75 B (No. 8) ribbons.

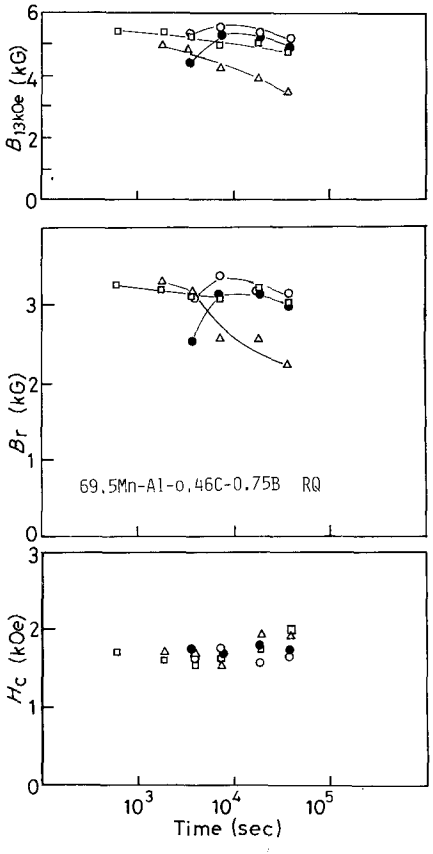

Figure 14 Relation between tempering time and magnetic properties of the rapidly quenched 69.5 Mn–Al–0.46 C–0.75B ribbons.

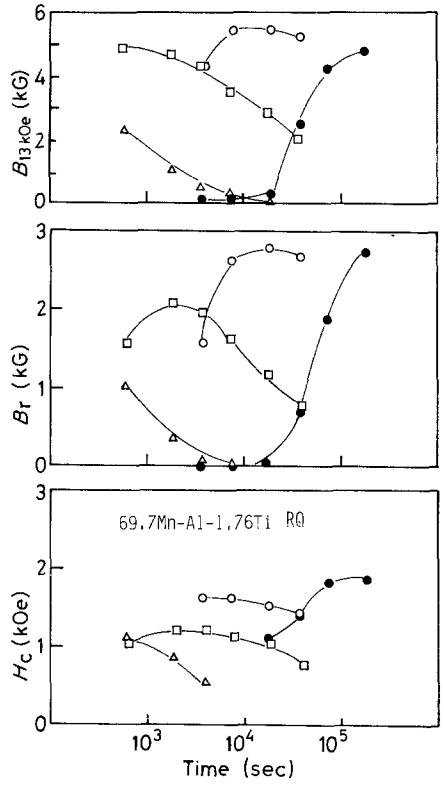

Figure 15 Relation between tempering time and magnetic properties of the rapidly quenched 69.7 Mn–Al–1.76 Ti ribbons.

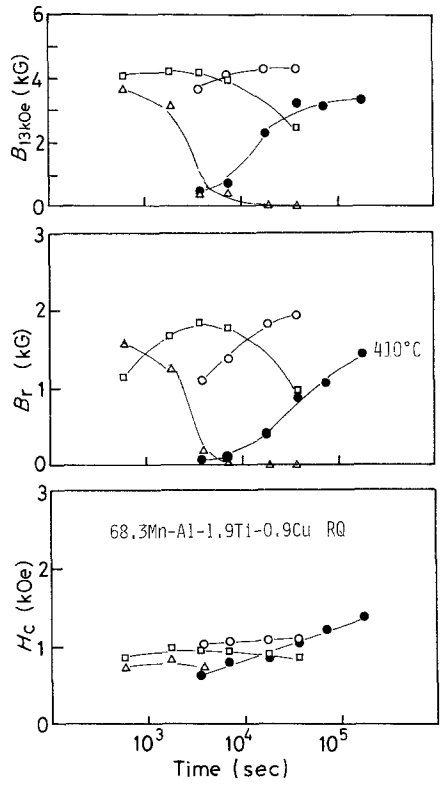

Figure 16 Relation between tempering time and magnetic properties of the rapidly quenched 68.3 Mn–Al–1.9 Ti–0.9 Cu ribbons.

Carbon doping seems able to increase the B_r in Mn–Al–B systems.

3.2.4. Mn–Al–Ti (Cu) systems

Figure 15 shows the relation between tempering time and magnetic properties of the rapidly quenched 69.7 Mn–Al–1.76 Ti (No. 9) ribbons. The transformation to π phase is depressed, and both Boron and H_c increased by doping titanium. Additional doping of copper (No. 10) was tried; however, the magnetic properties was not affected as shown in Fig. 16.

In the unit cell of the π phase of MnAl alloy, which has a body centred tetragonal structure, manganese occupy the (0 0 0) site and almost all aluminium and the excess manganese occupy the (1/2 1/2 1/2) site [14]. The magnetic moment of manganese occupied (0 0 0) sites is considered to be parallel to the c-axis and that of manganese occupied (1/2 1/2 1/2) sites is considered to be anti-parallel to the c-axis. The net magnetic moment is determined by the occupied site of the X atoms in Mn–Al–X systems. Carbon [15] and titanium [16] are considered to occupy (1/2 1/2 1/2) sites; however copper and nickel [16] are considered to occupy (0 0 0) sites. Since the unit cell of π phase of manganese occupied (1/2 1/2 1/2) sites is antiferromagnetic, the net magnetic moment is considered to be increased by doping carbon and titanium atoms which occupy the (1/2 1/2 1/2) sites and slightly decreased by doping copper and nickel. From above consideration, titanium and carbon doped Mn–Al samples may have relatively good hard magnetic properties, and nickel and copper doped samples may affect little hard magnetic properties.

Doping titanium retards the transformation of ε phase to π phase as seen in Fig. 15. The ε phase seems to be stabilized by titanium doping as is in the case of carbon, where carbide is precipitated; however, the existence of the titanium compound precipitate was not confirmed. To ascertain the transformation features of titanium doped alloy, more detailed microstructural observations are needed.

4. Conclusion

The Mn–Al–X rapidly quenched ribbons were fabricated in the conditions of a rotating iron (8 cm) roller speed of 6200 r.p.m. and an argon pressure of 0.6 kg cm^{-2}. The ribbons were quenched into the high temperature phase. The ribbons were brittle especially the carbon doped ones; however, the titanium doped ribbons were relatively ductile.

The rapidly quenched ribbons have a larger B_r and H_c than the water-quenched bulk samples in the Mn–Al systems. These results also applied to Mn–Al–C alloys where carbon contents were within the solubility limit. In the Mn–Al–C systems where the carbon content was beyond the solubility limit, however, the rapidly quenched ribbons and water-quenched samples showed similar magnetic properties and transformation features, probably owing to the Mn_3AlC precipitate. The phase transformations were retarded by the carbon doping beyond its solubility limit and titanium doping.

Carbon, titanium and boron doped ribbons showed relatively good magnetic properties. Mechanical properties take into consideration that titanium doped ribbons showed the best magnetic properties.

Acknowledgements

The authors wish to thank E. Furubayashi, Y. Kawabe, H. Maeda and M. Uehara for their helpful suggestions and discussions.

References

1. A. J. J. KOCH, P. HOKKELING, M. G. V. D. STEEG and K. J. De VOS, *J. Appl. Phys.* **31** (1960) 75S.
2. H. KONO, *J. Phys. Soc. Jpn* **13** (1958) 1444.
3. J. J. VAN Den BROEK, H. DONKERSLOOT, G. VAN TENDELOO and J. VAN LANDUYT, *Acta Met.* **27** (1979) 1497.
4. W. H. DREIZLER and A. MENTH, *IEEEE Trans. Mag.* **MAG-16** (1980) 534.
5. T. OHTANI, N. KATO, S. KOJIMA, K. KOJIMA, Y. SAKAMOTO, I. KONNO, M. TSUKAHARA and T. KUBO, *ibid.* **MAG-13** (1977) 1328.
6. S. KOJIMA, *J. Mag. Soc. Jpn* **6** (1982) 18.
7. Z. A. ABDELNOUR, H. F. MILDRUM and K. J. STRNAT, *IEEE Trans. Mag.* **MAG-17** (1981) 2651.
8. A. INOUE, T. MASUMOTO and H. TOMIOKA, *J. Mater. Sci.* **19** (1984) 3097.
9. R. H. WILLENS, *IEEE Trans. Mag.* **MAG-16** (1980) 1059.
10. M. TAKAHASHI and T. MIYAZAKI, *J. Mag. Soc. Jpn* **6** (1982) 22.
11. A. E. BERKOWITZ, J. D. LIVINGSTON and J. L. WALTER, *J. Appl. Phys.* **55** (1984) 2106.
12. T. KAWAGUCHI, M. NAGAKURA, K. KAMINO and S. YOSHIZAWA, *Nippon Kinzoku Gakkaishi* **28** (1964) 384.
13. K. KAMINO, *ibid.* **30** (1966) 636.
14. P. B. BRAUN and J. A. GOEDKOOP, *Acta Cryst.* **16** (1963) 737.
15. Y. YANG, W. HO, C. LIN, J. YANG, H. ZHOU, J. ZHU, X. ZENG, B. ZHANG and L. JIN, *J. Appl. Phys.* **55** (1984) 2053.
16. H. KANEKO, T. NISHIZAWA and M. HOMMA, *Nippon Kinzoku Gakkaishi* **31** (1967) 1331.
17. E. L. HOUSEMAN and J. P. JAKUBOVICS, *J. Mag. Mag. Mater.* **31–34** (1983) 1005.

Received 24 August 1988
and accepted 12 January 1989